Rayleigh–Brillouin scattering of carbon dioxide

Z. Y. Gu,[1] W. Ubachs,[1,*] and W. van de Water[2]

[1]*Department of Physics and Astronomy, LaserLaB, VU University, De Boelelaan 1081, 1081 HV Amsterdam, The Netherlands*

[2]*Physics Department, Eindhoven University of Technology, Postbus 513, 5600 MB Eindhoven, The Netherlands*

Corresponding author: w.m.g.ubachs@vu.nl

The spectral line shape of spontaneous Rayleigh–Brillouin scattering in CO_2 is studied in a range of pressures. The spectrum is influenced by the bulk viscosity η_b, which is a relaxation phenomenon involving the internal degrees of freedom of the molecule. The associated relaxation rates can be compared to the frequency shift of the scattered light, which demands precise measurements of the spectral line shape. We find $\eta_b = (5.7 \pm 0.6) \times 10^{-6}$ kg m^{-1} s^{-1} for the range of pressures $p = 2$–4 bar and for room temperature conditions.   © 2014 Optical Society of America

OCIS codes: (290.5830) Scattering, Brillouin; (290.5840) Scattering, molecules; (290.5870) Scattering, Rayleigh; (010.0010) Atmospheric and oceanic optics; (140.6810) Thermal effects.

http://dx.doi.org/10.1364/OL.39.003301

We present a study on the precise spectral shape of light that is quasi-elastically scattered off a gas of CO_2 molecules. The spectrum depends on the internal degrees of freedom of the molecule. For CO_2 the rotational relaxation rate, the rate of energy exchange between the translational and rotational degrees of freedom through collisions, is comparable to the frequency shift of the scattered light, while the vibrational relaxation rates are comparable to the megahertz frequencies of conventional ultrasound experiments. This makes an interesting case to test models of the spectral line shape using precise experiments. The relaxation of internal degrees of freedom determines the bulk viscosity η_b, which is a parameter in models of the line shape.

This study was inspired by a recent debate in the literature about the precise value of η_b of CO_2 [1]. It was made possible by the construction of a new experimental setup which provides spectra with unprecedented statistical accuracy [2]. Accurate information about the spectral line shape of Rayleigh–Brillouin backscattered light is of relevance for remote sensing applications in the Earth atmosphere [3] as well as for oceanographic applications [4]. In particular, detailed information is needed for ESA's future ADM-Aeolus mission, which will provide global observations of wind profiles from space utilizing an active satellite-based remote sensing instrument in the form of a Doppler wind lidar [5]. Information on scattering from CO_2 is of relevance for investigations of the atmospheres of Venus and Mars where carbon dioxide is the main constituent.

Rayleigh–Brillouin scattering is caused by spontaneous density fluctuations: sound. The spectral line shape of the scattered light is influenced by the damping of sound through the molecular viscosity of the gas. If the gas consists of molecules with internal degrees of freedom, such as rotation or vibration, the viscosity is also influenced by the relaxation of these freedoms. For CO_2 at atmospheric pressures, the relaxation time for rotational motion τ_r is $\tau_r = 3.8 \times 10^{-10}$ s, while for vibrational motion it is $\tau_v = 6 \times 10^{-6}$ s [6]. The relaxation of internal modes of motion determines the bulk viscosity η_b. At low sound frequencies f in the range of megahertz, both rotational and vibrational modes couple with translation, and η_b is large, $\eta_b = 1.46 \times 10^{-2}$ kg m^{-1} s^{-1};

however, in light scattering experiments, the typical period of sound is $\mathcal{O}(10^{-9}$ s), which is much shorter than τ_v, so that the vibrational modes are frozen, and the bulk viscosity is reduced dramatically. This was noticed by Lao *et al.* [7], and again by Pan *et al.* [1] in the context of coherent Rayleigh–Brillouin scattering. Lao *et al.* found $\eta_b = 4.6 \times 10^{-6}$ kg m^{-1} s^{-1}, while Pan *et al.* found $\eta_b = 3.7 \times 10^{-6}$ kg m^{-1} s^{-1}. In coherent Rayleigh–Brillouin scattering, density variations are induced by dipole forces by crossing laser beams. Spontaneous Rayleigh–Brillouin scattering and coherent Rayleigh–Brillouin scattering share the same statistical description of the scattered light spectrum, and both can be used to determine the bulk viscosity at hypersound frequencies. However, coherent scattering results in a large increase of the scattered light intensity [8,9]. Note also that the scattering spectral lines shapes in the coherent and spontaneous forms of Rayleigh–Brillouin scattering are markedly different, therewith providing independent means to determine the bulk viscosity of a gas.

Our spontaneous Rayleigh–Brillouin scattering experiments are in the kinetic regime, where the inverse scattering wave vector can be compared to the mean free path between collisions. This regime is characterized by a nonuniformity parameter, $y = \mathcal{O}(1)$, where y is defined as $y = p/(kv_0\eta) = nk_BT/(kv_0\eta)$, with k the scattering wave vector, n the number density, k_B the Boltzmann constant, T the temperature, p the pressure, v_0 the thermal velocity, $v_0 = (2k_BT/M)^{1/2}$, with M the mass of the molecular scatterers, and η the (shear) viscosity. Accordingly, the Boltzmann equation must be used to describe the scattered light spectrum. In the Tenti model the collision integral of the linearized Boltzmann equation is approximated with the Wang Chang and Uhlenbeck approach, using six (S6) or seven (S7) moments [10,11].

We revisit the bulk viscosity of CO_2 and present scattered light spectra of CO_2 for pressures $p = 1$–4 bar. In order to extract the bulk viscosity from the spectrum, the measured Rayleigh–Brillouin scattering spectra are compared to spectra predicted using the Tenti models, with η_b used as a fit parameter. Since the bulk viscosity is a relaxation parameter, and since the mean free time between collisions is inversely proportional to pressure, we expect a (slight) dependence of η_b on pressure.

From a straightforward extension of the arguments in [12], the frequency-dependent bulk viscosity can be related to the relaxation time of the internal degrees of freedom,

$$\eta_b = 2nk_BT \left| \frac{\sum_j N_j \tau_j (1 + i\omega\tau_j)^{-1}}{N(3 + \sum_j N_j(1 + i\omega\tau_j)^{-1})} \right|, \qquad (1)$$

where N_j is the number of internal degrees of freedom with relaxation time τ_j, $N = 3 + \sum_j N_j$ is the total number of degrees of freedom, n the molecular number density, and where it is assumed that the internal degrees of freedom do not interact with other ones having a different relaxation time, and the density is small. When the frequency of sound waves $\omega = 2\pi f$ is much larger than $1/\tau_j$, the mode j remains frozen and does not contribute to the bulk viscosity. On the other hand, when ω is much smaller than all relaxation rates, Eq. (1) reduces to the relation [12]

$$\eta_b = 2nk_BT \sum_j N_j \tau_j / N^2. \qquad (2)$$

Since an increase of the pressure results in an increase of the collision rates thus a decrease of the relaxation time of internal modes of motion, and since the sound frequency and the relaxation time appear in the combination $\omega\tau_j$, we expect that the bulk viscosity *increases* with increasing pressure.

The interpretation of η_b as a relaxation parameter is not without controversy [13]. Here we use η_b as a parameter in a kinetic model for the scattered light line shape. In the context of a continuum description, Meador *et al.* [13] also arrive at an equation expressing η_b in terms of a relaxation time, which they deem incomplete. Similarly, also Eq. (1) cannot be complete as it still contains the multiplicity N_j of frozen modes for which $\omega\tau_j = \infty$.

A schematic view of the setup used for spontaneous Rayleigh–Brillouin scattering is shown in Fig. 1, with a detailed description provided in [2]. Briefly, the light
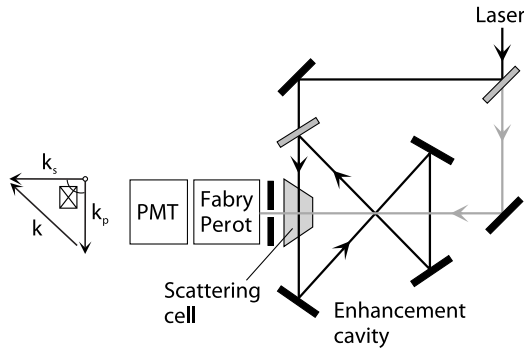

Fig. 1. Schematic diagram of the experimental setup for spontaneous Rayleigh–Brillouin scattering (not to scale). The UV laser beam (full black line) is reflected several times in the enhancement cavity to increase the scattering intensity. A reference beam (gray line), split off the main beam, is used for detector alignment. Scattered light is detected at 90° using a pinhole, a Fabry–Perot interferometer, and a photomultiplier (PMT).

from a narrowband continuous-wave laser is scattered off the CO_2 gas contained in a temperature-controlled gas cell. The laser is a frequency-doubled Ti:Sa laser delivering light at 366.8 nm, 2 MHz bandwidth, and 500 mW of output power. The long-term frequency drift was measured with a wavelength meter to be smaller than 10 MHz per hour. The scattered light is collected at an angle of 90° from an auxiliary focus inside an enhancement cavity, in which a scattering cell is mounted. The cell is sealed with Brewster windows. The circulation of the light inside the enhancement cavity amplifies the power by a factor of 10. A hemispherical scanning Fabry–Perot interferometer (FPI) is used to resolve the frequency spectrum of the scattered light. The drift of the laser frequency is much smaller than the drift of the FPI, with both drifts being corrected for by a frequency linearization procedure. All experiments were performed in CO_2 gas at $T = 296.5 \pm 0.5$ K.

The spectral response $S(f)$ of the FPI was measured in a separate experiment, and could be parametrized very well by the formula

$$S(f) = \{1 + [(2f_{FSR}/\pi f_w) \sin(\pi f/f_{FSR})]^2\}^{-1}, \qquad (3)$$

where f_{FSR} is the free spectral range (FSR) of the FPI, $f_{FSR} = 7440$ MHz, and $f_w = 232$ MHz is the Airy-width of the transmission peak. All computed model spectra were convolved with $S(f)$, and since the FSR is relatively small, it is important to allow for the periodic nature of $S(f)$. The light that passes through the FPI is detected using a photomultiplier tube (PMT), which is operated in the photon-counting mode and read out by a computer.

The experimental and computed spectra were normalized such that $\int_{-f_b}^{f_b} I(f)df = 1$, where the integral extends over one FSR, $f_b = f_{FSR}/2$. In addition, the background of the model spectra was fitted to the experimental data. An estimate of the χ^2 error was obtained assuming Poissonian statistics of the photon counts.

The results are shown in Fig. 2. We fit the bulk viscosity η_b in both Tenti S6 and S7 models and find the values for η_b, which minimize the χ^2 difference between model and experiment. As Fig. 2(e) indicates, the minimum of χ^2 is well defined at high pressures where the Brillouin side peaks are pronounced, and not very well defined at $p = 1$ bar. We find significant systematic differences between the model and the experiment, corresponding to large values of χ^2. These differences are also shown in Figs. 2(a)–2(d). The model-Brillouin peaks appear shifted toward larger (absolute) frequencies compared to those of the experiment. The position of the Brillouin peaks represents the velocity of sound, which is determined by the internal degrees of motion of the molecule. It is tempting to vary the heat capacity of internal motion in order to obtain a better fit. At these frequencies only rotations should partake in the relaxation of the internal energy, with the heat capacity of internal motion $c_{int} = 1$. A slightly better fit of the peak locations could be obtained by setting $c_{int} = 1.16$, but now discrepancies at other frequencies become more obvious. Therefore, we kept $c_{int} = 1$, while we used $\eta = 1.46 \times 10^{-5}$ kg m^{-1} s^{-1} for the shear viscosity and $\kappa = 1.31 \times 10^{-2}$ WK^{-1} m^{-1} for the thermal conductivity [1].
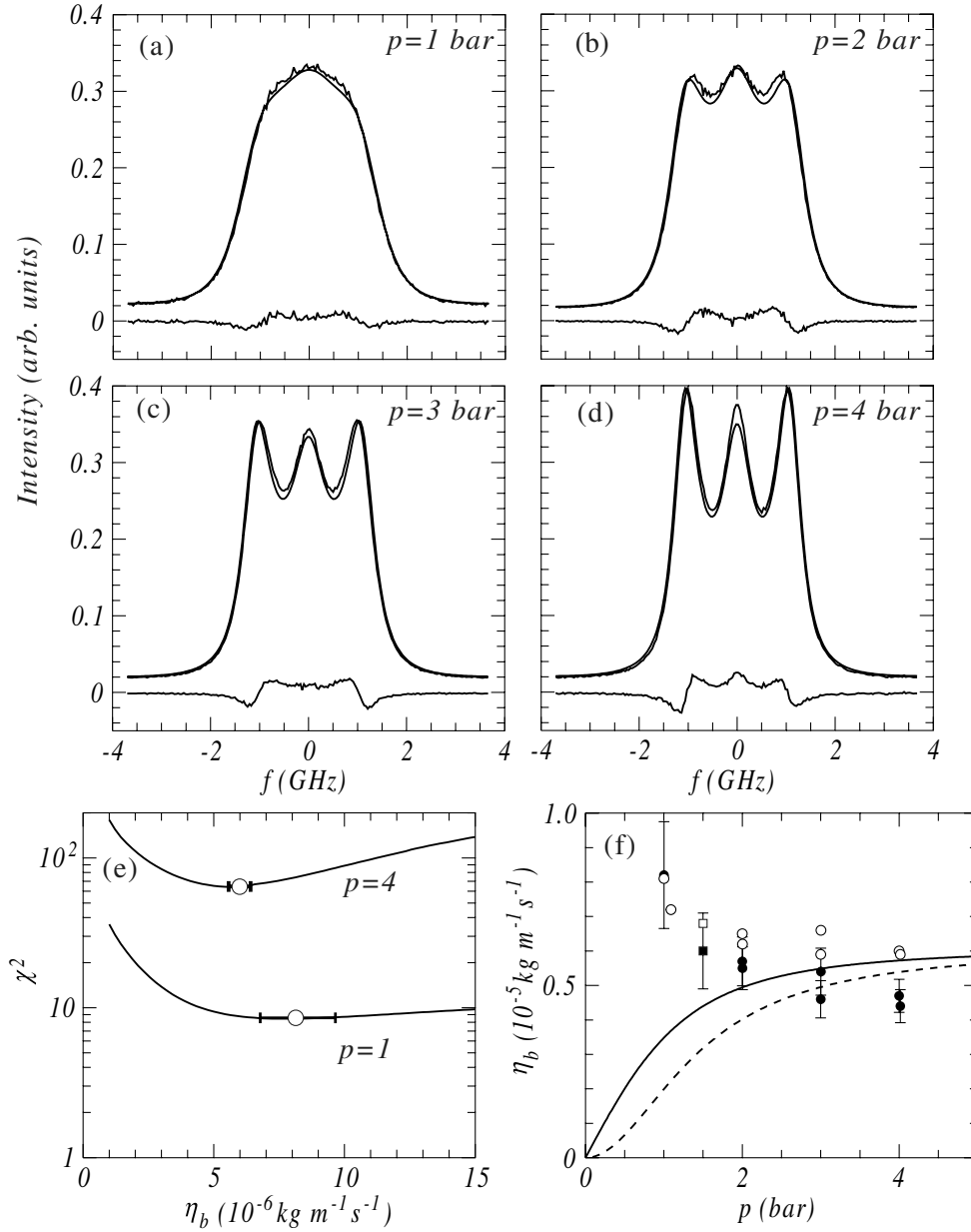
Fig. 2.   (a)–(d) CO_2 Rayleigh–Brillouin scattering spectra at pressures $p = 1, 2, 3,$ and 4 bar and for conditions of 296.5 ± 0.5 K. The spectra are shown together with the Tenti S7 model; the lower line indicates the difference between the model and experiment. The model calculations include a convolution with the instrument function of the FP-analyzer. The used bulk viscosities are indicated by the open symbols in frame (f). (e) Lines are χ^2 differences between the experimental spectra and the Tenti S7 model as a function of η_b, the open balls indicate the minimum χ^2. (f) Symbols indicate the bulk viscosity obtained by fitting the Tenti model to the experimental spectra. Dots are for the Tenti S6 model, open balls are for the Tenti S7 model. Full line: prediction using Eq. (1) with two rotational degrees of freedom and relaxation time $\tau_r = 3.8 \times 10^{-10}$ s. The dashed line represents the prediction of Eq. 28 in [13]. The points at $p = 1.5$ bar (indicated with filled squares for an analysis with Tenti S6 and open squares for Tenti S7) were measured using 403.0 nm laser light, and an FP-analyzer with $f_{\mathrm{FSR}} = 7553$ MHz, and $f_w = 139$ MHz. To avoid congestion, only the error bars for the S6 model are shown, those of the S7 model are roughly the same.

The measured bulk viscosities are shown in Fig. 2(f), which collects the results of two experimental runs recorded at $\lambda = 366.8$ nm, taken a few months apart and an additional measurement recorded at $\lambda = 403.0$ nm and $p = 1.5$ bar. The uncertainties in the derived values for η_b are composed of three contributions. The typical contribution of the statistical uncertainty, as a result of the fitting procedure shown in Fig. 2(e), is 5×10^{-8} $\mathrm{kg\,m^{-1}\,s^{-1}}$. The 0.9° uncertainty in the determination

of the scattering angle translates into a systematic uncertainty of typically 5×10^{-7} $\mathrm{kg\,m^{-1}\,s^{-1}}$, while the 1% uncertainty in the pressure reading corresponds to a contribution of 2×10^{-7} $\mathrm{kg\,m^{-1}\,s^{-1}}$. Here it is noted that for the lower pressures ($p \leq 2$ bar), where the information content of the spectrum is lower, all three contributions to the uncertainty are larger. At the highest pressure ($p = 4$ bar), where the effect of the bulk viscosity is most decisive, the total uncertainty is less than

5×10^{-7} kg m^{-1} s^{-1}. Further it should be noted that the systematic uncertainty of the determination of the scattering angle yields the largest contribution to the uncertainty budget, and that all measurements were performed in the same scattering geometry. Hence, the relative uncertainties are lower than the error bars indicated in Fig. 2(f).

For large pressures in the range $p = 2–4$ bar we obtain $\eta_b = (6.0 \pm 0.3) \times 10^{-6}$ kg m^{-1} s^{-1} using the Tenti S7 model and $\eta_b = (4.5 \pm 0.6) \times 10^{-6}$ kg m^{-1} s^{-1}. The measured η_b appear to *decrease* with increasing pressures, which does not agree with the simple idea that at finite frequencies ω, η_b should *increase* with increasing pressures, an idea which is embodied by Eq. (1). We compare the measured pressure dependence of η_b to the predictions of Eq. (1) and to Eq. 28 of [13] using a rotational relaxation time $\tau_r = 3.8 \times 10^{-10}$ s. These predictions disagree significantly with the experiments.

An averaged value of $\eta_b = (5.7 \pm 0.6) \times 10^{-6}$ kg m^{-1} s^{-1} for the bulk viscosity as obtained via the Tenti S6 and S7 models in the pressure range $p = 2–4$ bar can be compared to $\eta_b = 4.6 \times 10^{-6}$ kg m^{-1} s^{-1} by Lao *et al.* [7], and $\eta_b = (5.8 \pm 1) \times 10^{-6}$ kg m^{-1} s^{-1} by Meijer *et al.* using coherent Rayleigh–Brillouin scattering [9], but which is somewhat larger than the value $\eta_b = 3.7 \times 10^{-6}$ kg m^{-1} s^{-1} found by Pan *et al.* [1]. It is very different for light scattering experiments compared to acoustical experiments performed at megahertz frequencies. A problem is the significant difference between experiment and the Tenti models that were used to determine η_b. For our experiments on nitrogen gas at comparable pressures, the Tenti S6 model fits the data much better [14,15].

The core part of the code that computes the Tenti models has been kindly provided to us by X. Pan. Also,

References

1. X. G. Pan, M. N. Shneider, and R. B. Miles, Phys. Rev. A **71**, 045801 (2005).
2. Z. Y. Gu, M. O. Vieitez, E. J. van Duijn, and W. Ubachs, Rev. Sci. Instrum. **83**, 053112 (2012).
3. B. Witschas, C. Lemmerz, and O. Reitebuch, Opt. Lett. **39**, 1972 (2014).
4. K. Liang, Y. Ma, J. Huang, H. Li, and Y. Yu, Appl. Phys. B **105**, 421 (2011).
5. "ADM-Aeolus: Science Report," SP-1311 (ESA Communication Production Office, 2008).
6. J. Lambert, *Vibrational and Rotational Relaxation in Gases* (Clarendon, 1977).
7. Q. H. Lao, P. E. Schoen, and B. Chu, J. Chem. Phys. **64**, 3547 (1976).
8. X. G. Pan, M. N. Shneider, and R. B. Miles, Phys. Rev. A **69**, 033814 (2004).
9. A. S. Meijer, A. S. de Wijn, M. F. E. Peters, N. J. Dam, and W. van de Water, J. Chem. Phys. **133**, 164315 (2010).
10. C. D. Boley, R. C. Desai, and G. Tenti, Can. J. Phys. **50**, 2158 (1972).
11. G. Tenti, C. D. Boley, and R. C. Desai, Can. J. Phys. **52**, 285 (1974).
12. A. Chapman and T. G. Cowling, *Mathematical Theory of Non-Uniform Gases*, 3rd ed. (Cambridge Mathematical Library, 1970).
13. W. E. Meador, G. A. Miner, and L. W. Townsend, Phys. Fluids **8**, 258 (1996).
14. M. O. Vieitez, E.-J. van Duijn, W. Ubachs, B. Witschas, A. S. Meijer, A. S. de Wijn, N. J. Dam, and W. van de Water, Phys. Rev. A **82**, 043836 (2010).
15. Z. Y. Gu and W. Ubachs, Opt. Lett. **38**, 1110 (2013).